Optimization of Electrostatic Sensors for Rotational Speed Measurement of a Metallic Rotor

Xuanda Liu, Yong Yan, *Fellow, IEEE*, Yonghui Hu, *Senior Member, IEEE*, and Lijuan Wang, *Senior Member, IEEE*

***Abstract*— Previous studies have demonstrated that it is feasible to apply the electrostatic sensing technique for speed monitoring of nonmetallic rotating machinery. The attachment of electrostatic markers makes it possible to measure the rotational speed of metallic rotors with electrostatic sensors. The geometric shape and size of the electrodes and their spacing and distance to the rotor surface have a significant influence on the performance of electrostatic sensors. This article presents a scheme for the optimization of electrostatic sensors applied in the rotational speed measurement of a metallic rotor. Through computational modeling, the fundamental characteristics of the electrostatic sensor, including spatial sensitivity, output response, and frequency property, are analyzed; then, the optimal range of electrode parameters is obtained. An optimized sensor with double strip-shaped electrodes is used to measure the rotational speed of a metallic rotor with a triboelectric marker attached. Experimental results indicate that the electrostatic sensor coupled with correlation signal processing algorithms enables repeatable speed measurement of a metallic rotor, and the rangeability has been significantly extended. The system is capable of measuring the rotational speed as low as 30 r/min (revolution per minute) with a relative error within ±3.4% over the range of 30–120 r/min and within ±0.12% over the range of 120–3000 r/min.**

***Index Terms*— Electrode optimization, electrostatic marker, electrostatic sensors, metallic rotor, rotational speed.**

I. Introduction

ROTATIONAL machineries are widely used in industries, such as electric power, metallurgical, manufacturing, and many others. Most rotational machineries require continuous operation under harsh working conditions, which may lead to a gradual degradation in performance or even failure. Rotational speed is a key variable reflecting the operation condition of a mechanical system and holds great significance for condition monitoring [1], [2], fault diagnosis [3], and prognosis [4]. The accurate measurement of rotational speed is thus important in the control and regulation processes of mechanical systems.

Common techniques for rotational speed measurement are primarily based on mechanical, optical [5], [6], and electrical [7] principles. Each of these sensing techniques has its own limitations, such as low accuracy, limited rangeability, mechanical wear, susceptibility to harsh environments, high cost, and so on. In recent years, electrostatic sensors have attracted considerable attention in the field of industrial process monitoring because of their advantages, including noncontact sensing, robustness, simple structure, low cost, and suitability for harsh industrial environments. Combined with correlation signal processing, frequency-domain analysis, and other methods, the electrostatic sensing technique has been applied to the condition monitoring of rotating machinery [8], [9] and translational machinery [10], [11] under both steady-state and transient-state conditions [12].

Electrostatic sensor arrays have been applied to achieve rotational speed measurement, demonstrating high accuracy and repeatability. Double-electrode sensors outperform single-electrode sensors in terms of rangeability and reliability, making them more suitable for practical applications [13]. Electrostatic sensors have been applied to measure the rotational speed of a nonmetallic rotor [14], but there is limited research on metallic rotors to date. Because of the electrical conductivity of a metallic rotor, electrostatic sensors alone do not produce any useful signals for rotational speed measurement, limiting the applicability of electrostatic sensors in industry. Preliminary research aiming to measure the vibration displacement of a metallic rotor has been reported, where triboelectric markers are stuck on the rotor surface [15]. Adding markers on rotating targets presents a new approach to measure the rotational speed of metallic rotors. In addition, the optimization of electrostatic sensors plays a crucial role in improving signal quality, measurement accuracy, repeatability, and rangeability. Finite element modeling has been proven to be valid methods for quantifying sensing characteristics. In previous work [8], [12], [13], strip-shaped electrodes are used for rotational speed measurement of a nonmetallic rotor due to the fact that the electrostatic charge is distributed along the surface of the rotor—the strip-shaped electrode is in parallel with the rotor surface for maximum electrostatic induction and hence sensitivity. However, for a metallic rotor with a small triboelectric marker on its surface, which is very different from a nonmetallic rotor, the optimal shape and size of the electrodes are unknown. Moreover, the electrodes are part of a printed circuit board (sensor board), i.e., the electrodes should be flat. It is therefore essential to investigate the sensing characteristics of electrodes in different shapes and their optimal design for the given 3-D electrostatic sensing geometry (point

Manuscript received 31 July 2023; revised 4 November 2023; accepted 25 November 2023. Date of publication 13 December 2023; date of current version 29 December 2023. This work was supported by North China Electric Power University. The Associate Editor coordinating the review process was Dr. Yang Bai. *(Corresponding author: Yong Yan.)*

Xuanda Liu and Yonghui Hu are with the School of Control and Computer Engineering, North China Electric Power University, Beijing 102206, China (e-mail: liuxd@ncepu.edu.cn; huyhui@gmail.com).

Yong Yan and Lijuan Wang are with the School of Engineering, University of Kent, CT2 7NT Canterbury, U.K. (e-mail: y.yan@kent.ac.uk; l.wang@kent.ac.uk).

Digital Object Identifier 10.1109/TIM.2023.3342240

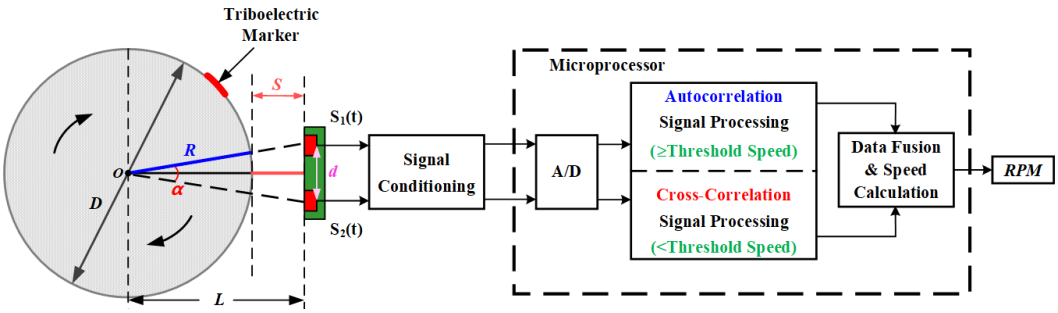

Fig. 1. Principle of the rotational speed measurement system for metallic rotors.

charge, conducting rotor, and flat electrodes). The sensing characteristics of strip and butterfly-shaped electrodes were studied by Reda et al. [16]; however, the optimization of electrode shape and its performance assessment are still a subject that requires further investigations. The optimal spacing between the two electrodes, which is related to the parameters of the data acquisition system, needs to be determined. Additionally, the electrostatic sensors to measure the speed of dielectric rotors as reported in previous studies [14], the minimum measurable speed is 100 r/min [13]. This limitation in rangeability makes the technique impractical or unreliable in low-speed scenarios. It is thus desirable to extend the lower limit of the range of rotational speeds.

This article presents an optimized design of electrostatic sensors for rotational speed measurement of a metallic rotor. The double-electrode sensor is optimized through theoretical analysis and computational modeling. By attaching a small triboelectric marker to the rotor surface, the sensor is capable of measuring the rotational speed of a metallic rotor. The optimization methodology of electrodes and preliminary results were initially reported at the 2023 International Instrumentation and Measurement Technology Conference [17]. This extended article provides a detailed description of the optimization strategy along with a resulting recommended range of key design parameters of the sensor and measurement system. The performance of the optimized sensor is assessed through a series of experimental tests.

II. Measurement Principle

The principle of rotational speed measurement through electrostatic sensing is the electrostatic induction between the electrostatic charge on the surface of the rotor and the electrode. Based on the triboelectric mechanism, the electrostatic charge will be generated on the surface of a moving object after contact and friction with the environmental medium. Thus, the effective operation of electrostatic sensors depends on the level of electrostatic charge on the rotor surface. However, the rotors of large rotating machines are mostly made of metals. Since the electrons inside the metal move freely, the electrostatic charge generated by the friction between the rotor surface and air is immediately transferred or neutralized by free electrons. This means that no induced charge is generated on the surface of the electrode during the rotation process. In this case, the electrostatic sensor does not give any useful signals. Therefore, to make the electrostatic sensor work for a metallic rotor, a dielectric marker with high charge affinity is attached to the surface of the rotor as a source charge. Subsequently, the rotational speed is obtained through correlation signal processing, which has been previously reported [8]. The principle of the rotational speed measurement system for metallic rotors is shown in Fig. 1. The measurement system consists of an electrostatic marker, a double-electrode electrostatic sensor, an associated signal conditioning circuit, a data acquisition unit, and a microprocessor.

Under ideal conditions, both autocorrelation and cross-correlation algorithms are used to determine the rotational speed over the full speed range. The rotational speed of the rotor is calculated from

$$\begin{cases} \mathrm{RPM}_{\mathrm{auto}} = \dfrac{60}{T} \\ \mathrm{RPM}_{\mathrm{cross}} = \dfrac{30\alpha}{\pi\tau} \end{cases} \tag{1}$$

where α is the central angle between the two electrodes, which is determined by the center-to-center spacing d between the electrodes. The signal period T and the transit time τ are determined from the locations of the dominant peaks in the autocorrelation and cross-correlation functions, respectively. T and τ are the most significant variables affecting the accuracy of speed measurement and depend on the sampling frequency and the data length in each measurement cycle.

Equation (1) shows that the rotational speed is inversely proportional to T or τ. To satisfy the reliability of the correlation algorithm for the speed measurement over the range from 0 to 3000 r/min, it is necessary to ensure the minimum T or τ is identifiable at the maximum rotational speed $\mathrm{RPM}_{\mathrm{max}}$. The lowest sampling frequency and minimum sampling period are assumed to be $f_{s\mathrm{min}}$ and Δt ($f_{s\mathrm{min}} = 1/\Delta t$), if T or τ is between $n\Delta t$ and $(n+1)\Delta t$, then the maximum error from the peak location of the correlation function is $\pm(1/2)\Delta t$. Hence, a relative error tolerance δ is defined to represent the allowable limit of error for T or τ, i.e.,

$$\delta = \pm\frac{\frac{1}{2}\Delta t}{n\Delta t} = \pm\frac{1}{2n}. \tag{2}$$

For autocorrelation and cross-correlation algorithms, the number of points n corresponding to T or τ is expressed as

$$\begin{cases} n_{\mathrm{auto}} = \dfrac{60}{\mathrm{RPM}_{\mathrm{max}}} \cdot \dfrac{1}{\Delta t} \\ n_{\mathrm{cross}} = \dfrac{30\alpha}{\pi \mathrm{RPM}_{\mathrm{max}}} \cdot \dfrac{1}{\Delta t}. \end{cases} \tag{3}$$

The maximum relative error of T or τ should be within the range of tolerance $|\delta|$, i.e.,

$$\begin{cases} \mathrm{RE}_{\mathrm{auto}} = \dfrac{\mathrm{RPM}_{\max} \cdot \Delta t}{120} \le |\delta| \\ \mathrm{RE}_{\mathrm{cross}} = \dfrac{\pi \cdot \mathrm{RPM}_{\max} \cdot \Delta t}{60\alpha} \le |\delta|. \end{cases} \tag{4}$$

Therefore, the lower limits of the sampling frequency required by the two algorithms are derived, respectively, from

$$\begin{cases} f_{\mathrm{auto}} = \dfrac{1}{\Delta t} \ge \dfrac{\mathrm{RPM}_{\max}}{120\delta} \\ f_{\mathrm{cross}} = \dfrac{1}{\Delta t} \ge \dfrac{\pi \mathrm{RPM}_{\max}}{60\alpha\delta}. \end{cases} \tag{5}$$

Equation (5) indicates that cross-correlation requires a higher sampling frequency than autocorrelation algorithm ($f_{\mathrm{cross}} > f_{\mathrm{auto}}$). Therefore, f_{cross} is regarded as the minimum required sampling frequency for the data acquisition system, which depends on the maximum rotational speed, the central angle between the two electrodes, and the relative error tolerance.

After determining the sampling frequency f_s, further analysis of the data length t_a is necessary. In order to satisfy the minimum requirements for both autocorrelation and cross-correlation algorithms, it is essential to ensure that at least one complete rotation period is included in the data length for the autocorrelation algorithm, and at least one transit time is included in the data length for the cross-correlation algorithm. It is recommended that the data length should be at least 2 times the maximum T or τ at the minimum speed ($\mathrm{RPM}_{\min}$), i.e.,

$$\begin{cases} t_{\mathrm{auto}} \ge 2T_{\max} = \dfrac{120}{\mathrm{RPM}_{\min}} \\ t_{\mathrm{cross}} \ge 2\tau_{\max} = \dfrac{60\alpha}{\pi \mathrm{RPM}_{\min}}. \end{cases} \tag{6}$$

It can be seen that the autocorrelation algorithm requires a longer data length ($t_{\mathrm{auto}} > t_{\mathrm{cross}}$). Consequently, t_{auto} should be considered as the lower limit of the data length for the data acquisition system.

In addition, experimental results in [18] have proven that the autocorrelation algorithm has higher accuracy, while the minimum measurable speed of the cross-correlation algorithm is much lower than that of autocorrelation. Hence, the combination of autocorrelation and cross-correlation algorithms is beneficial for improving measurement accuracy and extending the range of speed measurement. For a given data length, the minimum speed obtained from the autocorrelation algorithm should be used as the threshold for switching between the two algorithms. First, the rotational speed is calculated by the cross-correlation algorithm, and then, the speed is compared with the threshold. If the speed is lower than the threshold, the cross-correlation algorithm is used in the speed calculation. When the speed is greater than or equal to the threshold, the autocorrelation and data fusion algorithms are deemed more appropriate, i.e.,

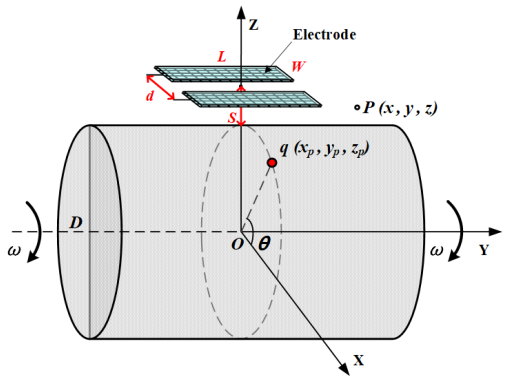

Fig. 2. Schematic of the electrostatic sensor model.

$$\mathrm{RPM}_{\mathrm{threshold}} = \mathrm{RPM}_{\mathrm{auto\,min}} = \frac{120}{t_{\mathrm{auto}}} \tag{7}$$

$$\mathrm{RPM} = \begin{cases} \mathrm{RPM}_{12}, & \mathrm{RPM}_{12} < \mathrm{RPM}_{\mathrm{threshold}} \\ \dfrac{c_1\mathrm{RPM}_1 + c_2\mathrm{RPM}_2 + c_{12}\mathrm{RPM}_{12}}{c_1 + c_2 + c_{12}}, & \\ & \mathrm{RPM}_{12} \ge \mathrm{RPM}_{\mathrm{threshold}} \end{cases} \tag{8}$$

where RPM_{12} and RPM_1 and RPM_2 are the measured rotational speeds using cross-correlation and autocorrelation algorithms, respectively, and c_{12} and c_1 and c_2 are the cross-correlation and autocorrelation coefficients, respectively.

III. Optimized Design of the Electrostatic Sensor

A. Finite Element Model

The physical model of the sensing system is composed of a metallic rotor, a small marker, and two electrodes. To study the interactions between the electrodes and the "point" marker and hence to optimize the electrode design, finite element modeling should be conducted. The charge density distribution on the surface being measured is determined based on the surface potential distribution and boundary conditions [11]. Since the potential distribution due to the rotating point charge is known, and when combined with finite element meshing, the charge distribution on the electrode surface is determined. As shown in Fig. 2, a point charge $q(x_p, y_p, z_p)$ is fixed on the surface of a rotor with a diameter D and rotating at an angular speed ω. The electrode is regarded as an ideal conductor with insulation and grounding. During the rotation process, electrostatic induction occurs between the source charge and the electrode; then, the induced charge is generated on the electrode surface.

For the model of a point charge, the potential at any position is contributed by both the point charge and the induced charge on the electrode surface. The potential at an arbitrary observation point $P(x, y, z)$ in space is expressed as

$$\varphi(P) = \frac{1}{4\pi\varepsilon_0}\left(\frac{q}{r} + \int_A \frac{\sigma_S}{r_e} dA\right) \tag{9}$$

$$r = \sqrt{(x - x_p)^2 + (y - y_p)^2 + (z - z_p)^2} \tag{10}$$

where q and σ_s are the quantity of the point charge and the induced charge density on the electrode surface, respectively. r is the distance between P and the point charge, and r_e is the distance from P to the induced charge. r_e depends on factors such as the shape and size of the electrode and the distance of the electrodes from the rotor surface.

For irregular-shaped electrodes, the boundaries cannot be determined by mathematical formulas. Hence, to solve (9), the finite element method is employed to obtain spatial position information for electrodes with various shapes. The electrode surface is divided into m grids, and the area of the ith grid is A_i. When the number of grids is large enough, the potential and the distribution of induced charge inside the grids are regarded as uniform. Therefore, the potential in grid j on the surface of the grounded electrode is given by

$$\varphi_j = \frac{1}{4\pi\varepsilon_0}\left(\frac{q}{r_{qj}} + \sum_{i=1}^{m}(\sigma_s)_i \int_{A_i}\frac{1}{r_{ij}}dA\right) = 0 \tag{11}$$

where r_{qj} is the distance from the point charge to the center of the jth grid, and r_{ij} is the center-to-center distance from grid i to j. Then, the matrix equation is obtained as follows:

$$\boldsymbol{\sigma_s} = -\boldsymbol{\varphi_q} \cdot \boldsymbol{P}^{-1} \tag{12}$$

where $\boldsymbol{\varphi_q}$ is the potential matrix of the point charge at each grid, $\boldsymbol{\sigma_s}$ is the matrix of induced charge density on the electrode surface, and $\boldsymbol{P}$ is the corresponding potential coefficient matrix; any of these elements P_{ij} is defined as

$$P_{ij} = \begin{cases} \dfrac{A_i}{4\pi\varepsilon_0 r_{ij}}, & i \neq j \\ \dfrac{r_i}{2\varepsilon_0}, & i = j. \end{cases} \tag{13}$$

Then, the charge density distribution $\boldsymbol{\sigma_s}$ is obtained by solving (12). The total amount of induced charge on the electrode surface $Q(t)$ and the output response $I(t)$ during the rotation process are determined, respectively, from

$$Q(t) = \sum_{i=1}^{m}\left[(\sigma_S)_i \times A_i\right] \tag{14}$$

$$I(t) = \frac{dQ(t)}{dt}. \tag{15}$$

Finally, the spatial sensitivity and frequency response of electrostatic sensors are calculated to quantify the sensing characteristics.

B. Optimization of Electrodes

1) Shape of Electrodes: The shape and size of the electrode affect the distribution of the spatial sensing volume. It is logical to initially determine the optimal electrode shape under identical constraints and subsequently optimize its size for a given rotor diameter. In order to elucidate how the electrostatic sensor responds to the circular motion of the point charge (the marker), the induced charge distribution at any time on the electrode is obtained from the finite element model. In this study, four different electrode shapes, including strip, rhombus, butterfly, and dumbbell [see Fig. 3(a)], are modeled. These four shapes have significant geometric differences between them and are hence considered. The area and central width of each shape are set to be equal [16]. Grids are divided for each shaped electrode; then, the spatial coordinates, dimensions, and the number of grids are acquired [see Fig. 3(b)].

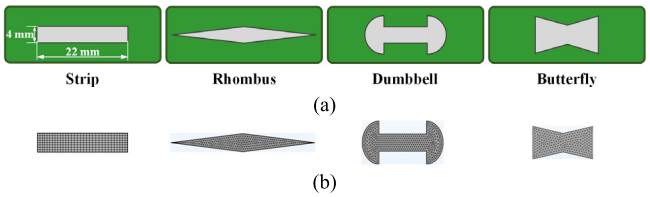

Fig. 3. Electrode shapes and their finite element models. (a) Different shaped electrodes. (b) Meshing of the models.

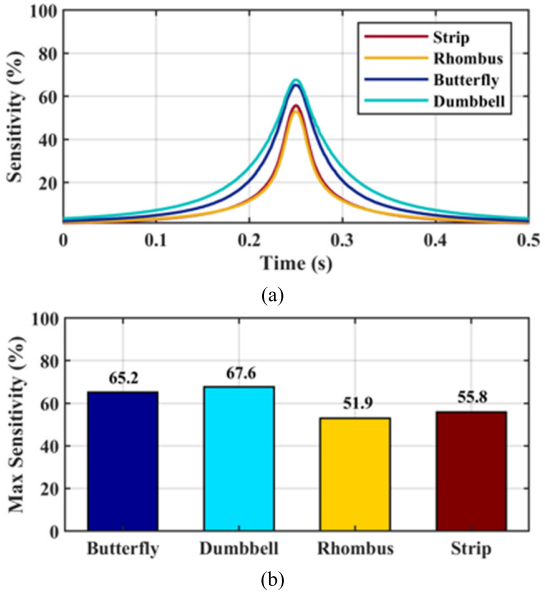

Fig. 4. Comparison of spatial sensitivity for different shaped electrodes. (a) Spatial sensitivity distribution. (b) Maximum spatial sensitivity.

Since the geometric parameters of the electrode are related to the diameter of the rotor (D), they are all normalized with reference to D. The normalized central width of each shape is set as $W/D = 1/15$, and the distance between the electrodes and the rotor surface is assumed to be $S/D = 1/30$. The angular speed of the point charge is $\omega = 2\pi$ rad/s. The potential coefficient matrix $\boldsymbol{P}$ is calculated according to the grid parameters, and the quantity of induced charge and output response at any time are obtained by solving (12). The spatial sensitivity, output response, power spectral density, and signal bandwidth during the rotation process of a point charge are depicted in Figs. 4–6, respectively.

It is evident that butterfly-shaped and dumbbell-shaped electrodes have good performance in terms of spatial sensitivity, but the output response and signal bandwidth are seriously low. This is due to their area being more concentrated near the center, resulting in a larger spatial sensing volume and a narrower signal frequency range than others. In addition, the subtle difference at the electrode boundary has little effect on the sensing characteristics. In view of the requirements of sensor design and fabrication, the strip-shaped electrode with good performance both in spatial sensitivity, output response

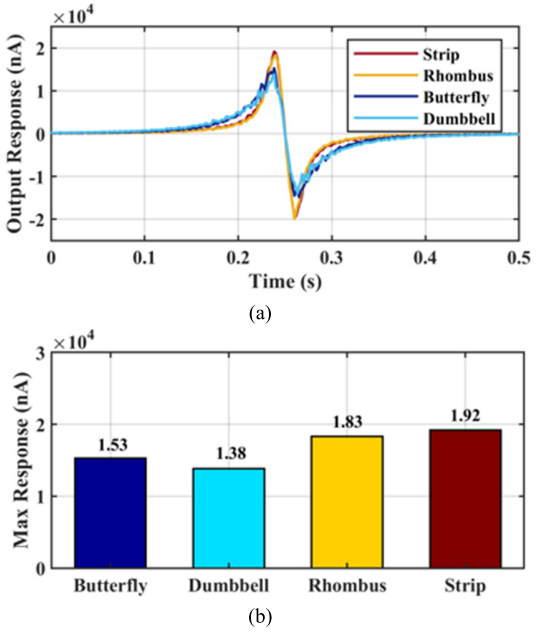

Fig. 5. Comparison of output response for different shaped electrodes. (a) Output response. (b) Maximum output response.

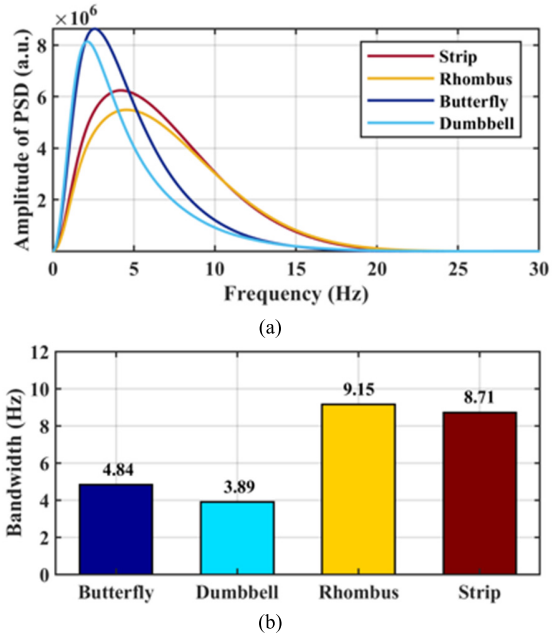

Fig. 6. Comparison of frequency properties for different shaped electrodes. (a) Power spectrum distribution. (b) Bandwidth.

and signal bandwidth, is regarded as the optimal electrode shape.

2) Size of Electrodes: The influence of electrode size on the sensing characteristics needs to be further studied. The grid numbers (m) and sensing distances (r_{ij} and r_{qj}) depend on the size of the electrode. Based on the control variate method [18], the normalized length and distance to the rotor surface of the electrode are set to be constant ($L/D = 2/5$ and $S/D = 1/30$), and the sensing characteristics are quantified from the developed model when the normalized width (W/D) changes from 0 to 1/2. The variations in spatial sensitivity, output response, and bandwidth with W/D are shown in Fig. 7.

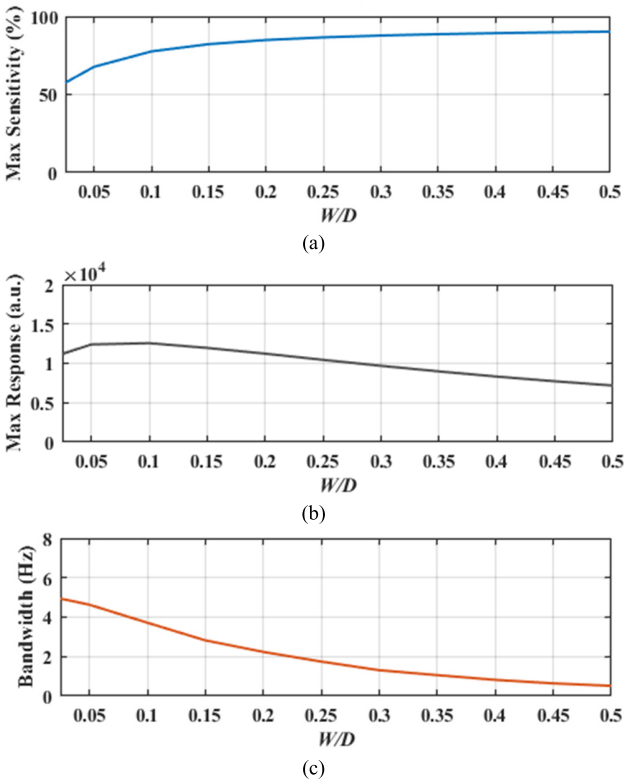

Fig. 7. Dependence of sensing characteristics on electrode width. (a) Maximum spatial sensitivity. (b) Maximum output response. (c) Signal bandwidth.

Similarly, when the normalized width is assumed to be constant ($W/D = 1/15$), the spatial sensitivity, output response, and bandwidth are obtained when L/D varies from 0 to 1, as shown in Fig. 8.

Fig. 8 shows that a small variation in electrode width leads to a significant change in sensitivity (57.58%–90.27%) and bandwidth (4.94–0.52 Hz). The sensing characteristics are more dependent upon the electrode width than its length, but the effect of the length cannot be ignored. The increase in spatial sensitivity is accompanied with reduction in bandwidth, so the decision of the optimal size needs to reach a tradeoff. Additionally, as the electrode size increases, more induced charge is accumulated on the electrode surface through electrostatic induction. This is also the reason why the maximum output response (gradient of the induced charge quantity) increases initially and then decreases. To achieve high spatial sensitivity and bandwidth for the electrostatic sensor, it is recommended that the optimal electrode width should be within the range of $(1/20)D$–$(3/20)D$ and the optimal length within $(1/10)D$–$(1/2)D$.

3) Distance of the Electrodes From the Rotor Surface: In the same way, when the normalized size of the electrode constant ($W/D = 1/15$ and $L/D = 11/30$) is kept constant, the model is used to analyze the influence of the distance (S) of the electrodes from the rotor surface on sensing characteristics. The sensing distance between the point charge and the electrode (r_{qj}) depends on S. As shown in Fig. 9, with the increase of S, the electric field strength weakens, so the spatial

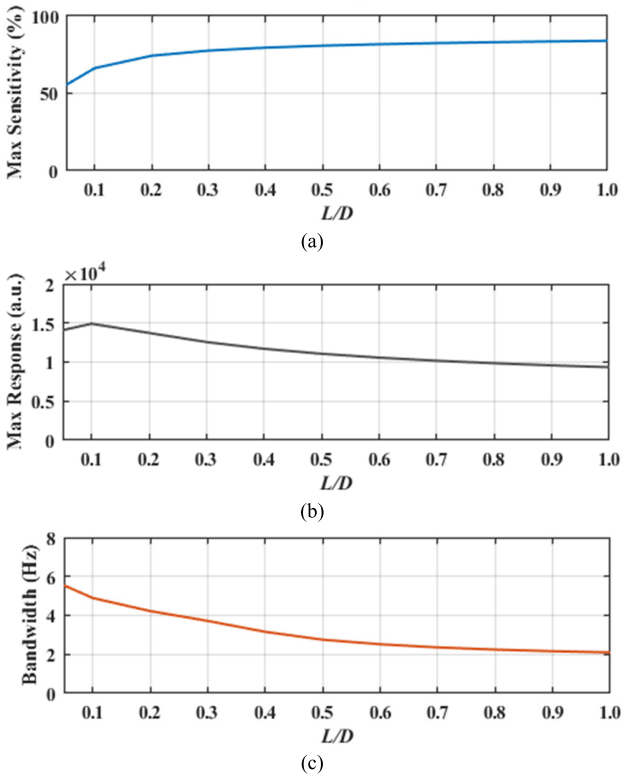

Fig. 8. Dependence of sensing characteristics on electrode length. (a) Maximum spatial sensitivity. (b) Maximum output response. (c) Signal bandwidth.

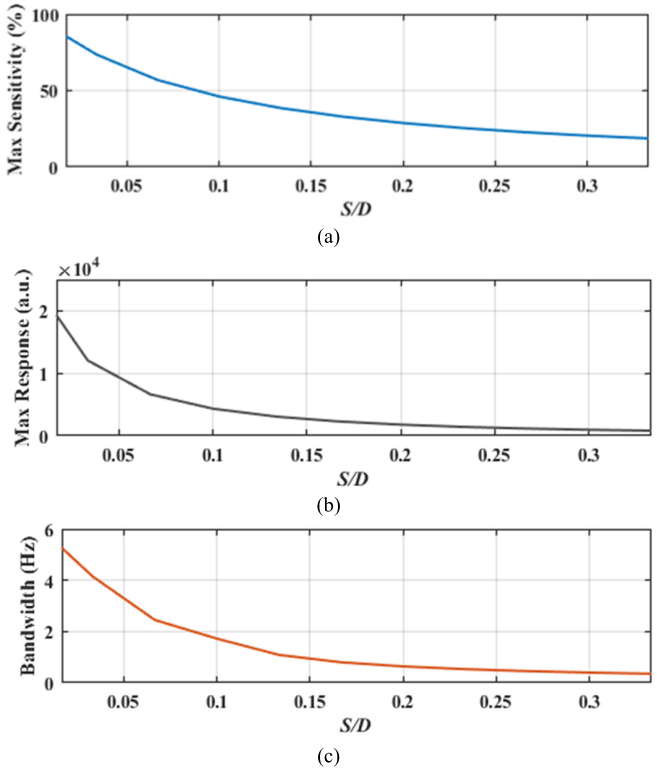

Fig. 9. Dependence of sensing characteristics on the distance of the electrodes from the rotor surface. (a) Maximum spatial sensitivity. (b) Maximum output response. (c) Signal bandwidth.

sensitivity, output response, and signal bandwidth decrease. The distance must be greater than the safe distance to avoid direct contact between the sensor and the rotor surface. Hence, the distance needs to be determined according to the operation condition of the rotor.

4) Spacing Between the Electrodes: The double-electrode electrostatic sensor has high reliability in rotational speed measurement by switching between autocorrelation and cross-correlation algorithms (see Section II). Meanwhile, it becomes possible with this design to extend the range of rotational speeds. However, a method for determining the optimized spacing between the two strip-shaped electrodes is desirable.

It is easy to understand that, with the increase of the spacing, the electrostatic charge on the rotor surface moves farther away from the center of the two electrodes (see Fig. 1), so the sensing distance becomes longer, resulting in the reduction in the spatial sensitivity, output response, and bandwidth. Therefore, the spacing between the two electrodes should not be exceedingly large. Furthermore, the lower limit of the spacing between the two electrodes primarily depends on the accuracy of the cross-correlation algorithm. As depicted in (16), any variation in the spacing (d) will lead to a change in the central angle (α) between the two electrodes, thereby indirectly affecting the resulting speed via cross-correlation

$$d = 2\left(\frac{D}{2} + S\right)\tan\frac{\alpha}{2}. \tag{16}$$

From (4), it can be observed that the maximum error of the cross-correlation algorithm occurs at the maximum rotational speed ($\mathrm{RPM_{max}}$). The relationship between τ and d/D at $\mathrm{RPM_{max}}$ is shown in Fig. 10.

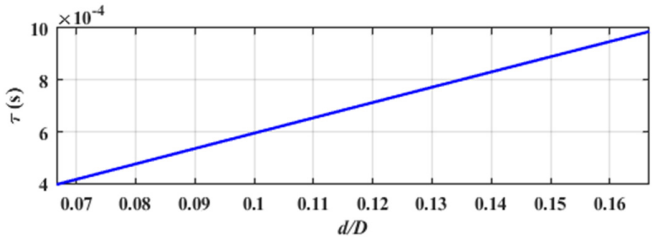

Fig. 10. Dependence of minimum transit time on the electrode spacing.

Equation (5) reveals that the spacing between the two electrodes is determined by the relative error tolerance (δ) and the lowest sampling frequency (f_{cross}) required by the cross-correlation algorithm. Then, the spacing is derived from

$$f_s \geq \frac{\mathrm{RPM_{max}}}{120\delta} \cdot \frac{\pi}{\arctan\left(\frac{d}{D+2S}\right)} \tag{17}$$

$$d \geq (D + 2S) \cdot \tan\left(\frac{\pi \mathrm{RPM_{max}}}{120\delta f_s}\right). \tag{18}$$

A smaller electrode spacing implies a shorter transit time between the upstream and downstream signals, requiring a sufficiently high sampling frequency to ensure higher measurement accuracy. Consequently, a smaller electrode spacing imposes greater demand on the sampling frequency. The electrode spacing should therefore be determined in conjunction with the sampling frequency. The relationship between the spacing and the sampling frequency is shown in Fig. 11, for

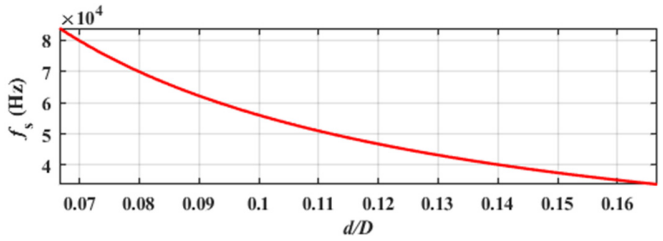

Fig. 11. Dependence of the lowest sampling frequency on electrode spacing.

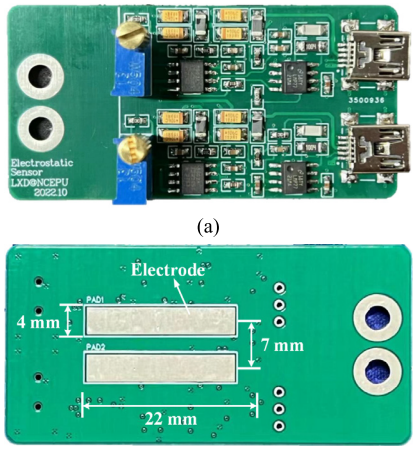

Fig. 12. Electrodes and sensor board. (a) Top preview. (b) Bottom preview (with electrodes).

given $W/D = 1/15$, $D = 60$ mm, and $\delta = \pm 1.5\%$. To avoid data redundancy caused by excessively high sampling frequency, a sampling frequency $f_s = 50$ kHz and a normalized spacing $d/D = 7/60$ are deemed appropriate.

IV. Experimental Results and Discussion

A. Sensor Design

Based on the optimization results of the electrodes (see Section III-B), the strip-shaped electrode is used as the optimal shape, with the optimal ranges for the width and length being $(1/20)D$–$(3/20)D$ and $(1/10)D$–$(1/2)D$, respectively, and the optimal spacing between the electrodes is $(7/60)D$. In the experimental study, a sensor board with double-strip-shaped electrodes is designed, as shown in Fig. 12. Since the diameter of the rotor on the test rig (see Section IV-B) is 60 mm, the width and length of the electrode are set to $(1/15)D = 4$ mm and $(11/30)D = 22$ mm, respectively, and the spacing between the electrodes is $(7/60)D = 7$ mm.

The sampling frequency and data length depend on the maximum speed to be measured, central angle between two electrodes, and relative error tolerance. In this study, the data length is set as $t_a = 1$ s, the maximum rotational speed is 3000 r/min, and the relative error tolerance is set to be $\delta = \pm 1.5\%$. From (5), for $d = 7$ mm and $\alpha = 0.218$ rad, then $f_{s\min} = 48\,063$ Hz. The sampling frequency is set to 50 kHz to meet the measurement requirements. The lower limits of the two algorithms are thus $\mathrm{RPM}_{\mathrm{automin}} = 120$ r/min and $\mathrm{RPM}_{\mathrm{crossmin}} = 4.16$ r/min, respectively, and the threshold speed for the algorithm switching of the correlation signal processing module is $\mathrm{RPM}_{\mathrm{threshold}} = 120$ r/min.

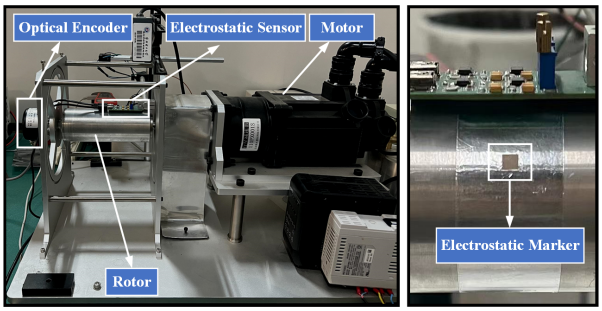

Fig. 13. (a) Test rig and the attached (b) marker on the rotor.

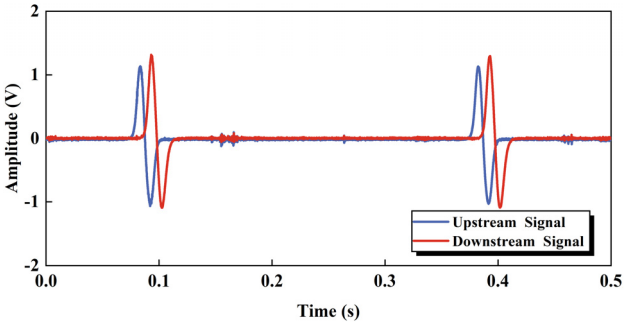

Fig. 14. Typical signal waveforms from the sensor.

B. Test Conditions

Experimental tests were conducted on a purpose-built motor test rig (see Fig. 13). The rotational speed is adjustable in a continuous range from 0 to 3000 r/min. The rotor is made of aluminum alloy with a diameter of 60 mm. The electrostatic sensor was placed $(1/30)D = 2$ mm away from the rotor surface, and the rotating speed of the rotor was measured. All the tests were conducted under an ambient temperature of 21 °C and relative humidity of 63%. An optical rotary encoder (Atonics, model E40H12) with a resolution of 2500 pulses per revolution (ppr) was used to obtain the reference speed and verify the measurement results.

C. Measurement Results

1) Signal Strength: The experimental results in [16] show that polytetrafluoroethylene (PTFE) has superior charge accumulation and retention capabilities compared to other common dielectric materials. In this study, a 130-μm-thick PTFE film of 2×2 mm is stuck to the rotor surface as a triboelectric marker. The marker is significantly smaller than the rotor and the electrodes. The rotational trajectory of the marker aligns with the center of the electrode. Figs. 14 and 15 show the typical signal waveforms from the electrostatic sensor and correlation functions at the speed of 200 r/min. It can be seen that the sensor outputs a pulse when the marker passes over the electrode. The periodicity of the signals and the time delay between them are clearly seen in Fig. 14.

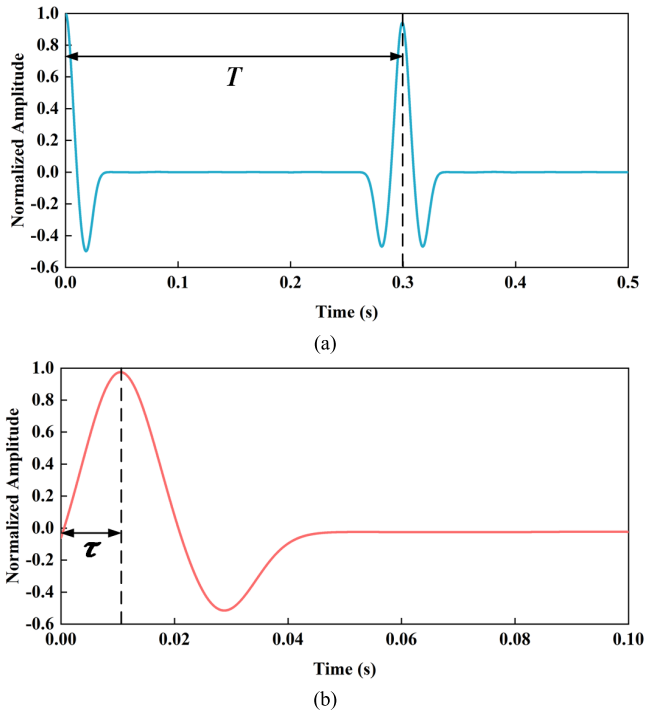

Fig. 15. Typical autocorrelation and cross-correlation functions. (a) Autocorrelation function. (b) Cross-correlation function.

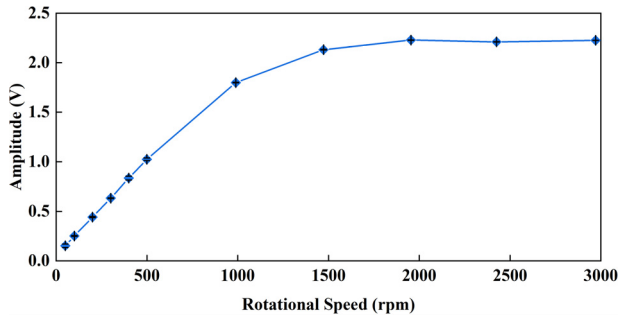

Fig. 16. Variation of the signal strength with rotational speed.

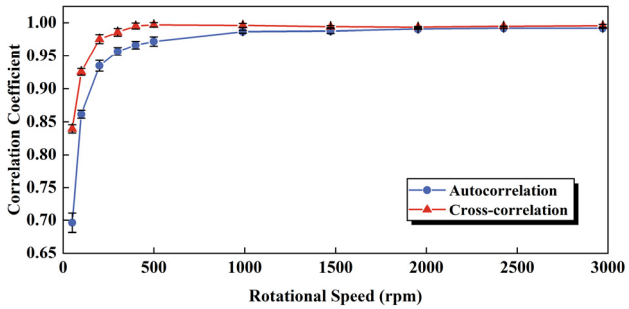

Fig. 17. Correlation coefficient of the two correlation algorithms.

The surface of the PTFE marker accumulates a lot of triboelectric charge during the rotation, resulting in a strong pulse output from the sensor. Unlike dielectric rotors [14], the metallic rotor produces no interfering electrostatic charge on its surface, and the output response exhibits a high signal-to-noise ratio. Fig. 15 depicts the autocorrelation and cross-correlation functions of the signals shown in Fig. 14. Then, the resulting signal period (T) and transit time (τ) are used to calculate the rotational speed from (1).

The pulse amplitude, i.e., the peak height (see Fig. 14), is used to quantify the strength of the signals. It can be seen from Fig. 16 that the triboelectric charge on the surface of the marker increases with the rotational speed, resulting in an increased rate of induced charge on the electrode surface, consequently, an increase in signal strength. The amplitude of the pulse signal is approximately 0.15 V at the rotational speed of 50 r/min and reaches 2.23 V at the maximum speed (3000 r/min). The signal strength saturates at approximately 2000 r/min, indicating that the charge accumulation on the surface of the marker reaches a constant value. At this point, the spatial electric field between the marker and the electrode reaches a dynamic equilibrium. Additionally, the strength of the signal depends on several other factors, including material type, surface roughness, and thickness of the marker, as well as environmental conditions. Further research is required to investigate these issues.

2) Correlation Coefficient: The autocorrelation coefficient reflects the periodicity of a signal, while the cross-correlation coefficient represents the similarity between two signals. The relationship between the correlation coefficients and the speed is shown in Fig. 17.

The results in Fig. 17 indicate that both the autocorrelation and the cross-correlation coefficients initially increase with the rotational speed and eventually reach the maximum. This is attributed to the increase in triboelectric charge on the marker at lower speeds (<500 r/min), which enhances the similarity between the two signals. When the speed is above 500 r/min, the charge on the marker is saturated, i.e., the charge density on the marker does not increase anymore with the speed. It is also noted that the cross-correlation coefficient drops slightly after 1000 r/min due likely to the slightly increasing vibration effect of the test rig at higher speeds (>1000 r/min). Since the transit time (τ) of the marker passing over the two electrodes is significantly shorter than the rotation period (T), the cross-correlation coefficient is consistently higher than autocorrelation coefficient throughout the speed range because of the better similarity between the two signals within a shorter period. At low speeds (<200 r/min), however, the autocorrelation coefficient goes below 0.93 due to the relatively low and unstable level of charge on the marker.

3) Accuracy: The accuracy of the measurement system is quantified in terms of relative error, which is determined from the measured speed against the reference speed. Each measured speed is an average of 30 repeated measurements. When the speed is above 120 r/min (the threshold speed), the speed is calculated using the data fusion algorithm [see (8)]. Fig. 18(a) shows a direct comparison between the measured and the reference speeds. The measured speed demonstrates a strong agreement with the reference speed.

Fig. 18(b) illustrates the relative error of the measured speed. The dashed lines delineate the range of the relative error. It can be seen that the relative error of the rotational speed measurement is within ±0.12% throughout the speed

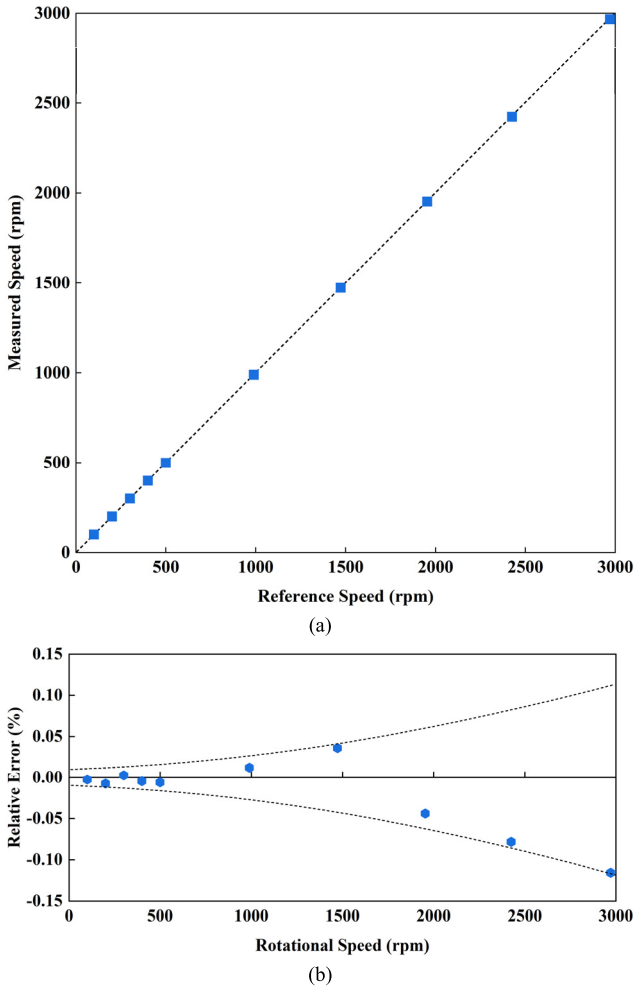

Fig. 18. Results of speed measurement (120–3000 r/min). (a) Comparison between measured and reference speeds. (b) Relative error of the measured speed.

range. The relative error increases with speed, which is consistent with (4). It is worth noting that the trend of relative error is opposite to that was found in previous studies on a nonmetallic rotor [14]. The reason for this is that, during the rotation of a metallic rotor with a marker attached, the sensor signals exhibit a higher signal-to-noise ratio (see Fig. 15). The relative error in this case is primarily attributed to the error in the determination of T or τ. For a given sampling frequency and a given data length, the number of sampling points corresponding to T or τ decreases with the speed, leading to reduction in the accuracy of T or τ determination and ultimately the measured rotational speed. At high rotational speeds (>2000 r/min), the mechanical vibrations of the rotor become more pronounced, leading to displacement of the encoder disk and the introduction of noise pulses [19], resulting in an overestimation of the pulse count and, consequently a slightly higher reference speed. This is believed to the reason for the consistently negative errors in Fig. 18(b) for speeds over 2000 r/min.

4) Repeatability: The repeatability of the measurement system is assessed using the normalized standard deviation. It can be observed from Fig. 19 that the normalized standard deviation of the measured rotational speed is not greater than

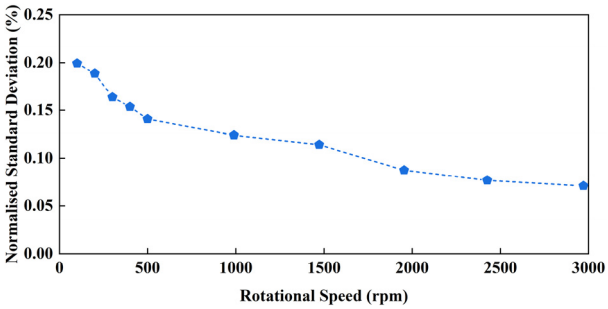

Fig. 19. Normalized standard deviation of the measured speed.

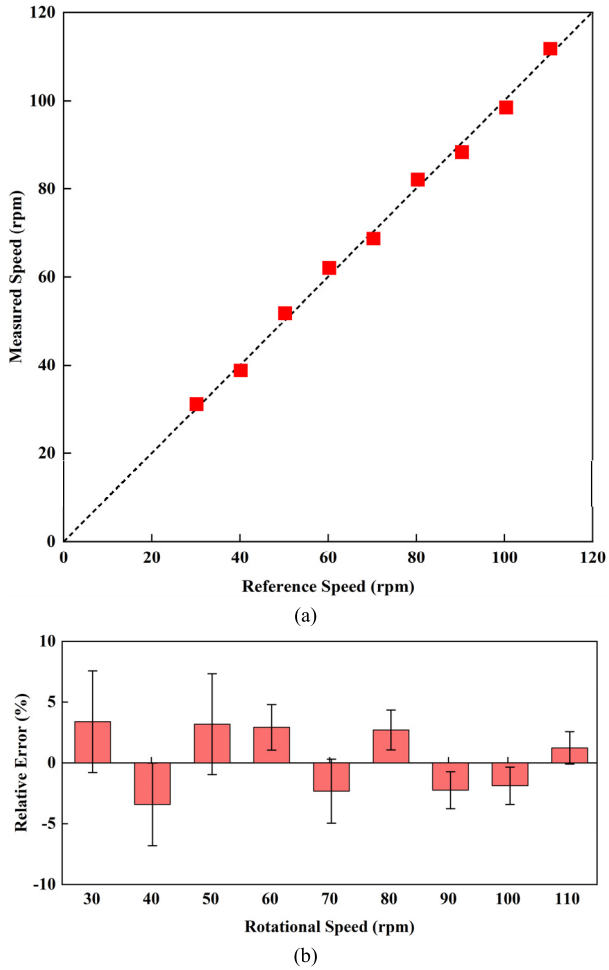

Fig. 20. Results of speed measurement (30–120 r/min). (a) Comparison between the measured and reference speeds. (b) Relative error of the measured speed.

0.2% over the speed range from 120 to 3000 r/min. It should be bore in mind that the results in Fig. 19 include the repeatability of the motor test rig. This means the actual repeatability of the measurement system is better than what is shown in Fig. 19. The repeatability of the system improves with increasing speed due to the increased accumulation of charge on the marker, leading to a more stable location of the dominant peaks in the correlation functions.

5) Measurement of Lower Rotational Speeds: A series of experiments were carried out for the speed range from 30 to 120 r/min in order to assess the performance of the

measurement system under low-speed conditions. If the actual speed is lower than the threshold speed, the cross-correlation algorithm is used to obtain the measured speed [see (8)]. Fig. 20 shows a direct comparison between the measured and the reference speeds and the resulting relative error, respectively, over the lower speed range.

With the use of the cross-correlation algorithm, the lowest measurable speed is reduced to 30 r/min with a relative error within ±3.4% and repeatability <4.1%. It is clear that the combination of autocorrelation and cross-correlation algorithms has extended the range of the speed measurement (30–3000 r/min). In addition, due to the use of the PTFE marker, its surface retains a certain level of electrostatic charge even at a very low rotational speed. This becomes another contributing factor that allows the system to achieve effective measurements of lower speeds.

It is worth noting that, when the rotational speed is below 120 r/min, the accuracy is not as high as the relative error tolerance (δ). In this case, signal quality is the most significant factor contributing to the measurement errors due to the lower amount of electrostatic charge on the marker as well as the fluctuation in charge level at lower speeds. As the speed increases, both signal stability and signal-to-noise ratio improve, resulting in improved accuracy and repeatability of the measurement results.

V. Conclusion

An optimization scheme of electrostatic sensors for rotational speed measurement of a metallic rotor has been proposed. The structural parameters of the electrodes, such as geometrical shape, size, distance to the rotor surface, and the spacing between the electrodes, have been analyzed numerically from the aspects of spatial sensitivity, output response, and frequency property through computational modeling. It can be concluded that the strip shape is the optimal electrode shape, the optimal width of the electrode is in the range of $(1/20)D$–$(3/20)D$, and the optimal length falls within the range of $(1/10)D$–$(1/2)D$. The distance between the electrodes and the rotor surface should be determined according to the operation condition of the rotor. The optimal spacing between the two electrodes should be $(7/60)D$ for $f_s =$ 50 kHz and $\delta = \pm 1.5\%$. The performance of the electrostatic sensor in measuring the rotational speed of a metallic rotor with a small dielectric marker on its surface has been assessed. Results obtained have demonstrated that the measurement system performs well over the range of 120-3000 r/min with a maximum error of ±0.12% and repeatability better than 0.2%. It is worth noting that the measurement range for rotational speed has been extended to include speeds as low as 30 r/min. The relative error in the rotational speed measurement is within ±3.4% over the range from 30 to 120 r/min with repeatability of <4.1%. Future research will include optimized design of the triboelectrification markers, including their shape, size, and distribution on the rotor.

References

[1] S. B. Lee et al., "Condition monitoring of industrial electric machines: State of the art and future challenges," *IEEE Ind. Electron. Mag.*, vol. 14, no. 4, pp. 158–167, Dec. 2020.

[2] Z. Wen, H. Zuo, and M. G. Pecht, "Electrostatic monitoring of gas path debris for aero-engines," *IEEE Trans. Rel.*, vol. 60, no. 1, pp. 33–40, Mar. 2011.

[3] Z. Duan, T. Wu, S. Guo, T. Shao, R. Malekian, and Z. Li, "Development and trend of condition monitoring and fault diagnosis of multi-sensors information fusion for rolling bearings: A review," *Int. J. Adv. Manuf. Technol.*, vol. 96, nos. 1–4, pp. 803–819, Apr. 2018.

[4] M. Hossain, A. Abu-Siada, and S. Muyeen, "Methods for advanced wind turbine condition monitoring and early diagnosis: A literature review," *Energies*, vol. 11, no. 5, p. 1309, May 2018.

[5] A. Bakibillah, M. A. Uddin, and S. A. Haque, "Design, implementation and performance analysis of a low-cost optical tachometer," *IIUC Stud.*, vol. 7, pp. 107–116, Oct. 2012.

[6] W. Li and J. Zhou, "Novel laser Doppler tachometer," *Chin. Opt. Lett.*, vol. 19, no. 1, 2021, Art. no. 011201.

[7] J. Pieniazek and P. Ryba, "Eddy-current sensor for a tachometer," *Trans. Aerosp. Res.*, vol. 2017, no. 2, pp. 57–68, Jun. 2017.

[8] L. Wang, Y. Yan, Y. Hu, and X. Qian, "Rotational speed measurement through electrostatic sensing and correlation signal processing," *IEEE Trans. Instrum. Meas.*, vol. 63, no. 5, pp. 1190–1199, May 2014.

[9] L. Li, X. Wang, H. Hu, and X. Liu, "Use of double correlation techniques for the improvement of rotation speed measurement based on electrostatic sensors," *Meas. Sci. Technol.*, vol. 27, no. 2, Dec. 2015, Art. no. 025004.

[10] Y. Hu, Y. Yan, L. Yang, L. Wang, and X. Qian, "Online continuous measurement of the operating deflection shape of power transmission belts through electrostatic charge sensing," *IEEE Trans. Instrum. Meas.*, vol. 66, no. 3, pp. 492–501, Mar. 2017.

[11] Y. Hu, S. Zhang, Y. Yan, L. Wang, X. Qian, and L. Yang, "A smart electrostatic sensor for online condition monitoring of power transmission belts," *IEEE Trans. Ind. Electron.*, vol. 64, no. 9, pp. 7313–7322, Sep. 2017.

[12] L. Wang, Y. Yan, Y. Hu, and X. Qian, "Intelligent condition monitoring of rotating machinery through electrostatic sensing and signal analysis," in *Proc. IEEE Int. Conf. Smart Instrum., Meas. Appl. (ICSIMA)*, Kuala Lumpur, Malaysia, Nov. 2013, pp. 1–4.

[13] L. Wang, Y. Yan, Y. Hu, and X. Qian, "Rotational speed measurement using single and double electrostatic sensors," *IEEE Sensors J.*, vol. 15, no. 3, pp. 1784–1793, Mar. 2015.

[14] L. Wang, Y. Yan, and K. Reda, "Comparison of single and double electrostatic sensors for rotational speed measurement," *Sens. Actuators A, Phys.*, vol. 266, pp. 46–55, Oct. 2017.

[15] K. Reda and Y. Yan, "Vibration measurement of an unbalanced metallic shaft using electrostatic sensors," *IEEE Trans. Instrum. Meas.*, vol. 68, no. 5, pp. 1467–1476, May 2019.

[16] K. Reda, Y. Yan, and L. Wang, "A comparative study of different shaped electrostatic sensors for rotational speed measurement," in *Proc. IEEE SENSORS*, Glasgow, U.K., Oct. 2017, pp. 1–3.

[17] X. Liu, Y. Yan, Y. Hu, and L. Wang, "Optimization of electrostatic sensors for rotational speed measurement," in *Proc. IEEE Int. Instrum. Meas. Technol. Conf. (I2MTC)*, Kuala Lumpur, Malaysia, May 2023, pp. 01–06.

[18] L. Wang and Y. Yan, "Mathematical modelling and experimental validation of electrostatic sensors for rotational speed measurement," *Meas. Sci. Technol.*, vol. 25, no. 11, Sep. 2014, Art. no. 115101.

[19] J. López, M. Artés, and I. Alejandre, "Analysis of optical linear encoders' errors under vibration at different mounting conditions," *Measurement*, vol. 44, no. 8, pp. 1367–1380, Oct. 2011.

Xuanda Liu received the B.Eng. degree in electrical engineering and automation and the M.Sc. degree in instrumentation science and technology from the North University of China, Shanxi, China, in 2018 and 2021, respectively. He is currently pursuing the Ph.D. degree in measurement technology and instrumentation with North China Electric Power University, Beijing, China.

His current research interests include electrostatic sensing, digital signal processing, and condition monitoring of mechanical systems.

Yong Yan (Fellow, IEEE) received the B.Eng. and M.Sc. degrees in instrumentation and control engineering from Tsinghua University, Beijing, China, in 1985 and 1988, respectively, and the Ph.D. degree in flow measurement and instrumentation from the University of Teesside, Middlesbrough, U.K., in 1992.

He was an Assistant Lecturer at Tsinghua University in 1988. In 1989, he joined the University of Teesside as a Research Assistant. After a short period of post-doctoral research, he was a Lecturer with the University of Teesside from 1993 to 1996, and then as a Senior Lecturer, a Reader, and a Professor with the University of Greenwich, Chatham, U.K., from 1996 to 2004. He is currently a Professor of electronic instrumentation and the Director of innovation with the School of Engineering, University of Kent, Canterbury, U.K. His current research interests include multiphase flow measurement, combustion instrumentation, intelligent measurement, and condition monitoring.

Dr. Yan was elected as a fellow of the Royal Academy of Engineering in 2020. He was awarded the Gold Medal in 2020 from IEEE TRANSACTIONS ON INSTRUMENTATION AND MEASUREMENT as the most published author of all time from U.K.

Yonghui Hu (Senior Member, IEEE) received the B.Eng. degree in automation from the Beijing Institute of Technology, Beijing, China, in 2004, and the Ph.D. degree in dynamics and control from Peking University, Beijing, in 2009.

He was a Post-Doctoral Research Fellow with Beihang University, Beijing, from 2010 to 2012, and a Research Associate with the University of Kent, Canterbury, U.K., from 2019 to 2021. He is currently an Associate Professor with the School of Control and Computer Engineering, North China Electric Power University, Beijing. His current research interests include multiphase flow measurement and condition monitoring of various industrial processes.

Lijuan Wang (Senior Member, IEEE) received the B.Eng. degree in computer science and technology from Qiqihar University, Xining, Heilongjiang, China, in 2010, and the Ph.D. degree in measurement and automation from North China Electric Power University, Beijing, China, in 2014 and the Ph.D. degree in electronic engineering from the University of Kent, Canterbury, U.K., in 2017.

She is currently a Lecturer in electronic engineering with the School of Engineering, University of Kent. Her current research interests include condition monitoring of mechanical systems, multiphase flow measurement, detection and measurement of waste plastics, smart sensors, and instrumentation systems.